# Numerical Simulation of Internal Self-Controlled Restrictor Hydrostatic Bearing with Discrete Oil Pocket Area

SONG Yanming, YANG Yang, ZHAO Gang

School of Mechanical Engineering and Automation, Beihang University, Beijing 100191, China

**Key words:** numerical simulation, pressure field, velocity filed, self-controlled restrictor hydrostatic bearing, discrete oil pocket area

**Abstract:** The computational fluid dynamics (CFD) method was used to establish the model of internal self-controlled restrictor hydrostatic bearing with discrete oil pocket area. The pressure field and velocity filed were calculated with different supply pressures and eccentricity ratios by the numerical simulation. The simulation results indicate that the load capacity of film increases with the supply pressure growing. The pressure in the lower oil pocket is larger than that in upper one. The flow also increases with supply pressure growing, but little relationship with the eccentricity. The bearing at the diameter of 200mm is designed and manufactured. The operation tests demonstrate that the pressure and velocity plot in the pocket is similar to the simulation one.

## 1 Introduction

Internal self-controlled restrictor hydrostatic bearing is placed in a fluid form bearing support within the bearing body, using the throttle gap with the outer surface of the spindle surface formed in the body of the fluid medium is throttled(Guo,2007). Because of the variable throttle ratio, making the self-controlled hydrostatic bearing has a large load capacity and high film rigidity. The simple restrictor hydrostatic bearing is increasingly used in high-precision machine tools and processing equipment(Yoshimoto,1993). Under large load situations, the use of an area ranging from the oil pocket structure will help improve the self-controlled hydrostatic bearing load capacity(Song,2014). In the design process of the oil film, bearing characteristics of complex structure calculations have some difficulty.

Under normal circumstances, supporting the theory of liquid and flow balance equation is used to calculate the basic hydrostatic bearing characteristics(Wang,2000; Makoto,2014). In recent years, scholar used CFD (Computational Fluid Dynamics) method(Savoldi,2013; Jiang,2011; Chen,2010) to calculated characteristics of simple structure the hydrostatic bearing. It is proved that the method had better visibility and accuracy. Gao(Gao,2014) used CFD method for water-lubricated hydrostatic bearing pressure of the flow field at different eccentricity. the distribution was calculated and experimentally verified the reliability of the calculation method. Based on CFD method, SONG(Song,2011) analyzed crankshaft connecting rod hydrostatic journal bearing to obtain a pressure contour and velocity vector distribution. Shao(Shao,2009) and Xu(Xu,2011) were used CFD method for the temperature field of heavy-duty hydrostatic bearing oil sector and a circular cavity simulation predictions. Wang Xinhua(Wang,2012) observed the 2D axis-symmetric flow model of the flow field characteristics of novel structure hydrostatic oil pads simulation analysis, calculating the internal flow field of new hydrostatic oil pads, oil pad bearing capacity and the stiffness of the film. Masaaki(Masaaki,2010) calculated aerostatic bearing static and dynamic characteristics of unconventional orifice mode using CFD.

In this paper, the CFD simulation analysis is used for the hydrostatic bearing oil film inside the complex feedback oil pocket with the structure of the film flow field area ranging from discrete area. The oil pocket and the boundary processing are set to give the corresponding. The oil film pressure field, velocity field situation are summed up capacity. The final test is carried out to verify the reliability of the calculation method, which adopted for the design of a variety of complex oil pocket structure.

## 2 Model

### *2.1 Physical Model*

The structure of the internal self-controlled hydrostatic bearing is shown in Figure 1. Spindle load suffered major gravity in the vertical direction, using the upper and lower oil pocket feedback throttling way into the oil. Since the horizontal force is relatively small, the use of orifice way is used.

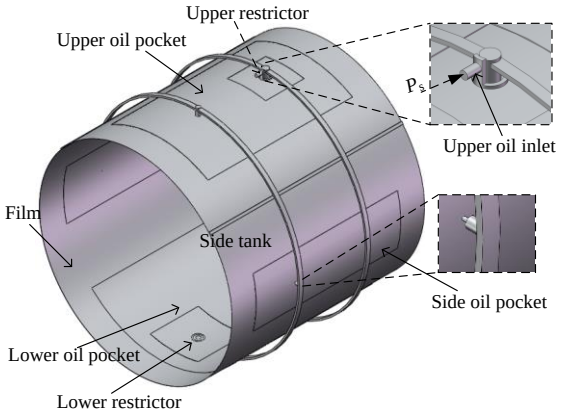


**Figure 1.** The film model of internal self-controlled hydrostatic bearing with unequal oil pocket area

$P_s$ supplied pressure oil is pumped through the main oil inlet into the throttle, into the working oil pocket through the feedback passage after throttling, the same as under the throttle on the working oil pocket is throttled oil. The oil finally is discharged through the back end surface of the oil sump and the oil film axial direction. The spindle load changes caused by the displacement of the spindle, the film will change the throttling gap, so that the upper and lower feedback oil pressure changes, to resist changes in load on the spindle.

In order to improve the load capacity in the vertical direction, so that the working oil pocket angle values ranging as large as possible within the permissible range, the basic structural parameters within the feedback oil pocket film unequal area as shown in Table 1.

**Table 1.** The basic structure parameters of the film

| **Parameters** | **value** |
|---|---|
| Diameter of the film | 200 mm |
| Angle of lower oil pocket | 130º |
| Angle of upper oil pocket | 80º |
| Angle of side oil pocket | 30º |
| Depth of oil pocket | 0.4 mm |
| Thickness of the film | 0.03 mm |
| Length of the film | 200 mm |

### *2.2 CFD model*

As can be seen by the physical model in figure1, the feedback area of the oil film has axis-symmetry structure. In order to simplify the model calculations, semi-film model is calculated. The model is meshed, as shown in figure 2. Since the film is extremely thin, with the return sump oil cavity size rank difference is more than $10^2$ times, the entire calculation area is divided into 19 separate areas meshing to improve convergence speed computing.

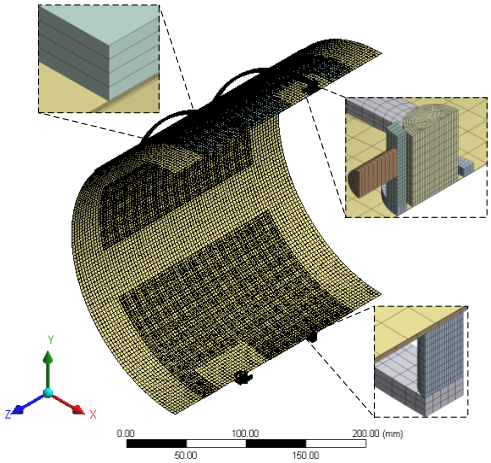


**Figure 2.** Half of the film meshing

According to the actual condition of the film, the upper and lower main oil inlet pressure at the inlet boundary condition to the boundary, and assign $P_s$=3 MPa, 3.5MPa, 4 MPa, 4.5 MPa, 5 MPa. The end and back axial side tank surfaces of the axial are the outlet boundary film pressure. The relative outlet pressure $P_{out}$ =0. The film and an inner wall surface and an outer surface of the contact surface of the spindle are set to no heat exchange. Steady implicit model calculation model is set to laminar flow. Fluid medium is 2# spindle oil, while the temperature $T$=298 K. this spindle oil density is 870 kg/m$^3$. And the dynamic viscosity is 0.00385 Pa•s.

All the boundary and conditions are set to the film, and then the simulation can be calculated.

## 3 Simulation results

### *3.1 Film pressure distribution*

Due to the different inlet pressure, distribution of film pressure field and trend different eccentricity under the same (different values) to eccentricity $\varepsilon$=0, $P_s$= 3 MPa as an example feature film pressure distribution, as shown in Figure 3.

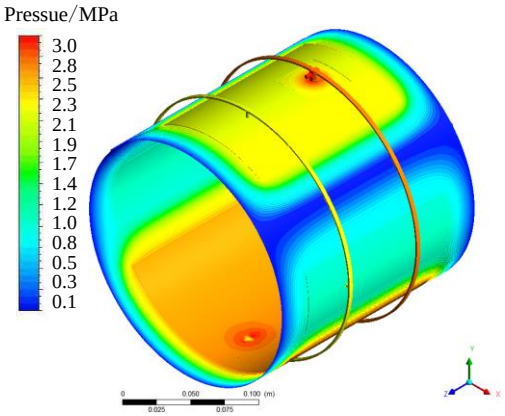


**Figure 3.** The film pressure distribution (ε=0,Ps=3 MPa)

As can be seen from the figure, the inlet throttling pressure is the higher location on the film. the side tank and axial end surfaces of the film are lower than others. The pressure inside the lower oil pocket is generally higher than that in the upper and the side pocket both. it is mainly that the feedback oil out from the lower oil pocket is distributed to the upper and both sides need to enter the working oil pocket, the restrictor feedback only working oil into the oil pocket and the side working oil pocket and the working oil pocket is greater than the effective area of the total area under the working oil pocket. Even on the pressure when the oil under the same restrictor, due to changes caused by the outlet area, the differences in the working oil pocket under pressure; the same time, we can see that the lower portion of the pressure side of the working oil pocket are higher than its upper pressure, which is due to the oil pocket arranged back to work on the tank, no

return to work under the oil sump pocket layout caused. Back to the sump and the oil film axial ends and the atmosphere, resulting in a return oil resistance decreases, while the bottom side of the working oil pocket of no return chute, end only through a very small gap back to the oil film axial direction, so that the oil return resistance increase large, this layout structure to some extent can enhance the carrying capacity of the oil film.

As can be seen in figure 4, under the same supplied pressure $P_s$, the oil film bearing load capacity is increasing with the eccentricity $\varepsilon$ up. Meanwhile, under the same eccentricity $\varepsilon$, the load capacity of the film would enlarge by the supply pressure growth.

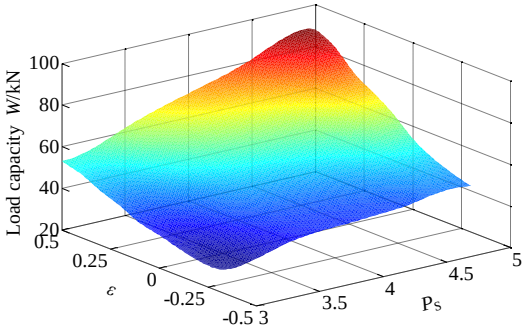


**Figure 4.** The film load capacity with different supply pressures and eccentricity ratios

### *3.2 Film velocity field*

The velocity field of the film can be obtained by calculating the distribution, as shown in Figure.5.

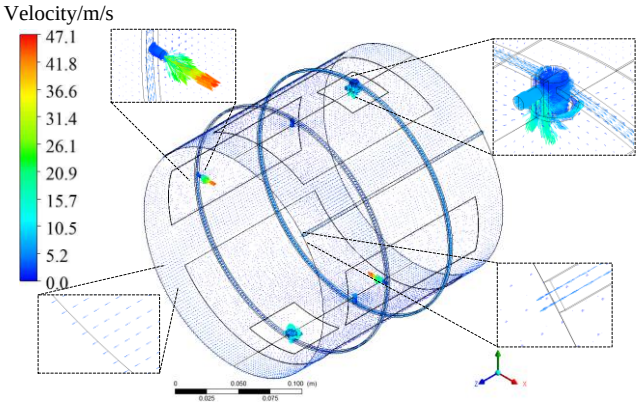


**Figure 5.** The film velocity distribution ($\varepsilon$=0, $P_s$=3 MPa)

Velocity profile can be more intuitive to see the work process within the self-controlled spindle oil throttling mode feedback. The spindle oil is pumped into the throttle, throttling after the throttling gap, gathering feedback to the feedback pocket through the oil sump into reverse 180º working oil pocket. The feedback oil into the side oil pocket via an orifice, since the cross section of the whole cut more intense, which caused here speed value appears steep, then appear the value of the maximum speed of the throttle orifice. It can be seen that enter spindle oil working oil pocket through the gap and the film back to the oil sump axial end, since a larger outlet area back to the fuel tank, fluid resistance small, back to the fuel tank at the outlet of the axial velocity was significantly higher than the oil film axial ends speed at the exit value.

## 4 Compared with test

According to the parameters of the bearing structure, the hydrostatic bearing system was manufactured and tested, as shown in figure 6.

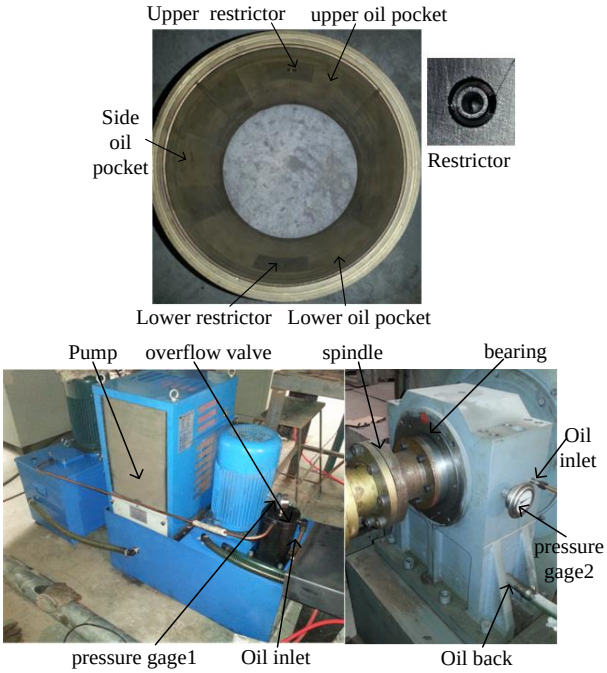


**Figure 6.** The hydrostatic bearing system

The pressure gage1 is test the oil supplied pressure $P_s$. The pressure gage2 is test the overall pressure in the lower oil pocket. The eccentricity $\varepsilon$ can be measured with different supplied pressure $P_s$ according to the value in simulation process. The load capacity in simulation $W$ and the real one can be compared. The relative errors can be summed in table 2.

It can be seen that the simulation of load capacity of the bearing is corresponding with the real one with a smaller real eccentricity. The trend of the numerical simulation results is similar to the actual measured.

**Table 2.** Relative errors of load capacity with different $P_s$

| $P_s$/(MPa) | $\varepsilon$ | $W$/(kN) | Relative errors |
|---|---|---|---|
| 3 | -0.03 | 33.9 | 5.3% |
| 3.5 | -0.17 | 33.9 | 5.3% |
| 4 | -0.30 | 37.9 | 17.7% |
| 4.5 | -0.40 | 37.7 | 17.1% |
| 5 | -0.47 | 38.1 | 18.3% |

## 5 Conclusions

By using CFD numerical simulation method, the complex structures internal self-controlled hydrostatic bearings with discrete oil pocket models were established and calculated, the pressure and velocity characteristics of the film were analyzed by pressure distribution and the flow field, the conclusions as followed:

(1) Increasing the inlet pressure, eccentricity help improve the bearing capacity.

(2) With the film flow into the oil pressure increases and growth, and minimal variation of eccentricity.

(3) The CFD method is useful in simulation of the complex contracture of self-controlled hydrostatic bearing.

## References

[1] Guo H S, Zhang J. Bearing **9** (2007)

[2] Yoshimoto S, Anno Y.J. Tri **115,** 2 (1993)
[3] Song Y M. Acta. A. A. S **35**, 4 (2014)
[4] Wang Y, Ma Y L. J. Harbin Tech **32**, 3 (2000)
[5] Makoto G, Kei S, Masaaki M.Trib. Int **75** (2014)
[6] L Savoldi R, R Zanino.Fu Eng. and D **88**(2013)
[7] Jiang Z H. J. B. Uni. of A.and A **37**, 12 (2011)
[8] Chen C Q. J. B. Uni. of A. and A **36**, 5 (2010)
[9] Gao G Y. Tri. Int **75** (2014)
[10] Song J C,Wang L. J.N.Uni **32**, 3(2011)
[11] Shao J P, J.Hydr 24, 1(2009)
[12] Xu X Q,Shao J P, Wang Y F. *IEEE* (2011)
[13] Wang X H, Cai L G,J. B. Uni. Tech **38**,1 (2012)
[14] Masaaki M, Shigeka Y. Tri.Int **43** (2010)